ACS APPLIED MATERIALS & INTERFACES

Research Article

www.acsami.org

Coal Oxide as a Thermally Robust Carbon-Based Proton Conductor

Kazuto Hatakeyama,*[,†] Chikako Ogata,[†] Michio Koinuma,[†] Takaaki Taniguchi,[‡] Shinya Hayami,[†] Keita Kuroiwa,[§] and Yasumichi Matsumoto*[,†]

[†]Graduate School of Science and Technology, Kumamoto University, 2-39-1 Kurokami, Chuo-ku, Kumamoto 860-8555, Japan

[‡]International Center for Materials Nanoarchitectonics (WPI-MANA), National Institute for Materials Science (NIMS), 1-1 Namiki, Tsukuba, Ibaraki 305-0044, Japan

[§]Department of Nanoscience Faculty of Engineering, Sojo University, 4-22-1 Ikeda, Nishi-ku, Kumamoto 860-0082, Japan

Supporting Information

ABSTRACT: Inexpensive solid proton conducting materials with high proton conductivity and thermal stability are necessary for practical solid state electrochemical devices. Here we report that coal oxide (CO) is a promising carbon-based proton conductor with remarkable thermal robustness. The CO produced by simple liquid-phase oxidation of coal demonstrates excellent dispersibility in water owing to the surface carboxyl groups. The proton conductivity of CO, 3.9×10^{-3} S cm^{-1} at 90% relative humidity, is as high as that of graphene oxide (GO). Remarkably, CO exhibits much higher thermal stability than GO, with CO retaining the excellent proton conductivity as well as the capacitance performance even after thermal annealing at 200 °C. Our study demonstrates that the chemical modification of the abundant coal provides proton conductors that can be used in practical applications for a wide range of energy devices.

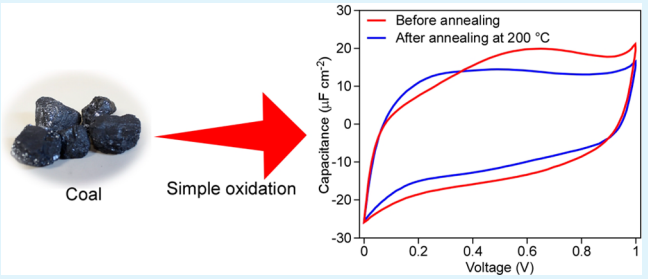

KEYWORDS: *carbon material, coal, proton conduction, solid state electrolyte, thermal stability*

1. INTRODUCTION

Covalent chemical modification of carbon-based nanomaterials is a versatile approach to tailor their functionalities. In particular, oxygenation is one of the most simple and effective processes to tune a wide range of properties of fullerene, carbon nanotubes, and graphene. For example, the oxidation of fullerene and carbon nanotubes gives rise to high water dispersibility as well as localized electric states that modify electronic and catalytic properties.[1,2]

Graphene oxide (GO), which is typically obtained via chemical oxidation of graphite flakes, has attracted a great deal of attention because of its easy production,[3] low cost,[3] and unique properties such as photoluminescence,[4,5] magnetism,[6,7] catalysis,[8,9] and molecular selectivity.[10−12] Recently, we have found that GO is an excellent proton conductor, adding a new functionality to those already known for GO. Following our finding, GO proton conductors have been intensively investigated to develop novel, inexpensive, and high-performance electrochemical devices.[13−15] However, unfortunately, GO is relatively unstable[16] so that oxygen functional groups such as the epoxide are decomposed by annealing at 100 °C or by application of a mild reducing agent.[17] This results in a drastic decrease of proton conductivity and an increase in the electron conductivity in these conditions,[17] presenting a serious barrier for practical applications of GO electrolyte membranes.

Here we investigate the use of coal as an alternative graphite source to develop a thermally robust carbon-based proton conductor. Coal is one of the oldest, most abundant, and most inexpensive fuels,[18] while the applications as multifunctional materials have been highly limited; the only example is the fabrication of graphene quantum dots by chemical treatment of coal.[19−21] In fact, so far, no studies have focused on the electrical and ionic transport properties of chemically modified coal as the functional properties. In this study, we demonstrate for the first time that, due to the high content of the carboxyl group, coal oxide (CO) produced by a simple liquid-phase oxidation method showed both high proton conductivity and high thermal stability; remarkably, CO retains its high proton conductivity and remains perfectly electrically insulating even after thermal annealing at 200 °C. Thus, the inexpensive and thermally robust CO proton conductor potentially exhibits a wide range of applications to develop practical electrochemical devices. In fact, we demonstrated that the all-solid-state electrochemical capacitor using the CO electrolyte (COEC) maintains its initial capacitance performance after thermal annealing at 200 °C. Also, like modified metal oxide nanoparticles,[22] nanosized CO would be efficiently hybridized with conventional proton exchange membranes to tailor their thermal stability.

Received: July 17, 2015
Accepted: October 5, 2015
Published: October 9, 2015

DOI: 10.1021/acsami.5b06470
ACS Appl. Mater. Interfaces 2015, 7, 23041−23046

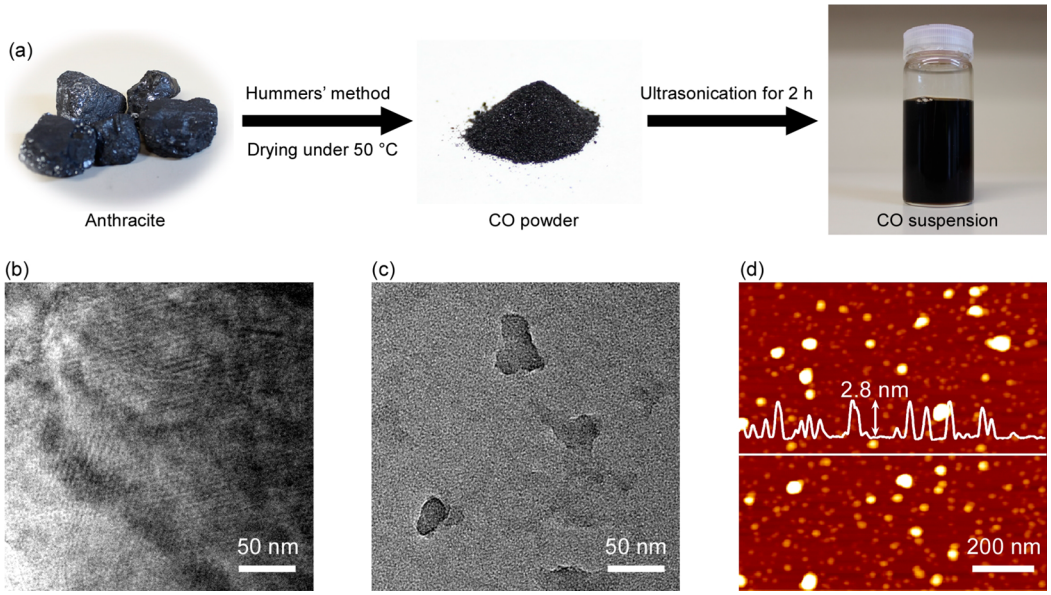

Figure 1. (a) Schematic for the fabrication of CO suspension. HR-TEM images of (b) anthracite and (c) CO. (d) AFM image of CO dried on mica.

2. EXPERIMENTAL SECTION

2.1. Materials. Coal oxide (CO) was prepared through the conventional Hummers' method[23] using anthracite (Sanyokosyo Co., Ltd., producing in Vietnam) pounded in a mortar, using $NaNO_3$, H_2SO_4, $KMnO_4$, and H_2O_2 solutions. The resulting mixture was washed several times with 5% HCl solution and distilled water and then dried in an oven (50 °C). The resultant CO powder was suspended in distilled water and sonicated for 2 h. To remove an insoluble impurity, the suspension was centrifuged and the supematant was collected. GO dispersion was prepared by the same method as CO using graphite powder (Wako Pure Chemical Industries Ltd.). Thermal annealing of the samples was performed using an oven (ETTAS, EO-300B) for 1 h.

2.2. Characterization. The morphologies of anthracite and CO powder were investigated by field-emission scanning electron microscopy (FE-SEM; Hitachi High-Tech, SU-8000). Atomic force microscopy (AFM; Bruker, Digital Instruments Nanoscope V) was used to examine the topography of the CO deposited on mica and Au comb electrode. A transmission electron microscope (TEM; FEI Co., Tecnai G2 F20) operating at 200 kV was used for determining the nanostructures of anthracite and CO. X-ray diffraction (XRD) data were collected via a Rigaku RINT2500 diffractometer using Cu Kα (λ = 0.154 nm). UV−vis spectra were obtained using a Jasco Japan V-550. X-ray photoelectron spectroscopy (XPS; Thermo Scientific, Sigma Probe) was performed to investigate oxygen functional groups (epoxy, hydroxy, and carbonyl groups) of CO and GO. Fourier transform infrared spectroscopy (FT-IR) data were recorded by an FT-IR spectrometer (PerkinElmer, Frontier IR/FIR) in the 600−4000 cm^{-1} frequency range using KBr pellets. Thermogravimetric analysis (TGA) curves were generated in a thermal analyzer (Seiko Instruments, EXSTAR 6000) at a scan rate of 4 °C min^{-1}. Raman spectra were recorded with a micro Raman spectrometer (Jasco Japan, NRS-3100) using a laser excitation line at 532 nm.

2.3. Electrochemical Analyses. Electrochemical characterization of CO and GO, including attenuation−correction (AC) analysis and cyclic voltammetry (CV), were measured by the two-probe method using the Au comb electrodes (width 2 μm, interval 2 μm, 65 pairs; BAS Ltd.). Note that the resistance of bare Au comb electrode is very high (>10^8 Ω). The samples for electrochemical analyses were prepared by drop-cast method. The proton conductivities (σ) of CO and GO were measured using an impedance/gain phase analyzer (Solartron 1260). The σ values were calculated using the formula $\sigma = L/(RTD)$, where R, L, T, and D refer to the proton conduction resistance, width, thickness, and length of the samples (Figure S1a). The details of the method for measurement and calculation of proton conductivities are described in Supporting Information. CV was carried out via a potentiostat and a function generator (Ivium Technologies, CompactStat) to evaluate the power capabilities of COEC and GO electrolyte (GOEC) at the scan rates of 0.01−1 V s^{-1}. The capacitance values were calculated by the following equation:

$$C_{device} = I/(dV/dt)$$

where I refers to the current in CV curves and dV/dt refers to the scan rate in CV measurement.

The areal capacitances of COEC and GOEC were calculated by the following equation:

$$C_A = C_{device}/A$$

A is the total area of the electrodes which touched with CO or GO obtained by the charge coupled device (CCD) measurement (Figures S1a and S2a).

3. RESULTS AND DISCUSSION

3.1. Synthesis of CO. In the present study, anthracite available in Vietnam was used for the production of CO. A schematic of the oxidation process is shown in Figure 1a. The conventional Hummers' method, which is well-known as the method for the production of graphite oxide, was employed as the oxidation process and CO powder was obtained. The FE-SEM images (Figure S3a,b) show that anthracite and CO powder have almost the same powder size, while edges of CO powder were rounded due to oxidation. The XRD pattern of anthracite (Figure S4) mainly shows the broad amorphous peak at a 2θ value around 25°. In addition, we observed a tiny sharp peak at 2θ = 26.5° corresponding to the graphitic layer distance of 0.34 nm. Thus, anthracite also includes graphite layers as a minor phase. TEM observation revealed that anthracite exhibits layered structures with a layer−layer distance of ∼5.5 nm. This suggests that, as well as oxidation of graphite flakes in Hummers' method,[24] oxidants can be inserted into interlayer space to oxidize the whole part of coal powder.

To prepare the CO colloid, the produced CO powder was suspended in distilled water by ultrasonication for 2 h followed by centrifugation to remove the insoluble matter. The resultant brown CO suspension (Figure 1a) has been stable at least for

DOI: 10.1021/acsami.5b06470
ACS Appl. Mater. Interfaces 2015, 7, 23041−23046

more than 6 months. The CO suspension exhibits an UV−vis absorption spectrum that is similar to that of the GO suspension (Figure S5). The AFM image (Figure 1d) of CO and the corresponding size distribution analysis (Figure S6) show that CO generally exhibits a plate or particulate shape with a width of ∼15−20 nm and a height of ∼2−3 nm. Notably, submicrometer or micrometer-sized sheets were not observed by AFM observation. This confirms that GO sheets formed from graphite phase were included insignificantly in the CO sample because of a tiny amount of graphite in an anthracite precursor. TEM observation of CO shows the presence of products with nanosized plate shapes, corresponding well to the AFM observation. Furthermore, TEM observation revealed that CO nanoplates are amorphous, likely due to the poorly crystalline nature of anthracite and/or due to introducing oxygen functional groups into anthracite. The XRD pattern of CO (Figure S4) also shows that CO is amorphous and never includes graphite or GO-like product. The entirely different structures of anthracite and CO demonstrate that the oxidation process occurs at the whole layer of anthracite.

The detailed analysis of oxygen functional groups was performed by XPS, and Figure 2 shows C 1s XPS spectra of the

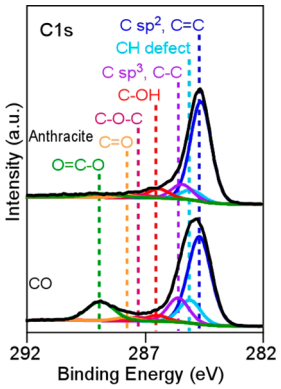

Figure 2. C 1s XPS spectra of anthracite and CO.

anthracite and CO. The deconvolution of the present XPS spectra, consisting of sp^2 C═C, C−H defect, sp^3 C−C, C−OH, C−O−C, C═O, and COOH bonds, was made following our previous report.[25] The C 1s XPS spectra of CO reveal that the CO contains carboxyl groups and that scarcely any other oxygen functional groups (epoxy, hydroxy, and carbonyl groups) are present. This feature was different from the case of GO, which mainly contains the epoxy groups. In general, the epoxy and hydroxy groups exist on the basal planes of GO, whereas the carboxyl groups are at the edges.[26] The unique structure of CO with only the carboxyl group is attributed to the fact that CO does not have a basal plane. This is another difference between CO and GO, which could offer thermal robustness to CO as demonstrated in the ensuing sections.

3.2. Proton Conduction of CO. Recently, the high proton conductivity of GO via its oxygen functional groups has been reported.[13,14,17] This allowed us to expect activation of proton conductivities by oxygen functional groups of coal. To test this hypothesis, we measured the proton conductivity of CO with the two-probe AC method using the Au comb electrode. Figure 3a represents the Nyquist plots of CO under various humidified conditions. The traces formed by the real (Z') and imaginary parts (Z'') of the impedance at each frequency were found to fit with distorted semicircular curves. Figure 3b shows the proton conductivities of CO and GO calculated from the Nyquist plots as a function of relative humidity (RH). The proton conductivities of CO were 1.4×10^{-5} and 3.9×10^{-3} S cm^{-1} at 40 and 90% RH, respectively. These values are almost the same as those for GO (2.7×10^{-5} and 2.5×10^{-3} S cm^{-1} at 40 and 90% RH, respectively). The temperature dependent proton conductivities from 20 to 80 °C are shown in Figure 3c, and the conductivities were found to increase with increasing temperature. Arrhenius plots (Figure 3d) revealed that the CO proton conduction activation energy (E_a) was 0.13 eV. The low E_a value implies that proton conduction in CO proceeds via the Grotthuss mechanism with protons moving by hopping from an H_3O^+ ion to the nearest water molecule.[27] Its high conductivity and low E_a for proton conduction are favorable for the use of CO in practical device applications. The faster proton movement in GO occurs via the interlayer water interacting with the epoxy group (Figure 3e).[13] Conversely, the proton transfer in CO is hypothesized to occur via the interface water trapped by the carboxyl group (Figure 3f).

3.3. Thermal Stability of CO. It has been widely accepted that the epoxy group in GO is easily decomposed, whereas the carboxyl group is rather stable for a range of reducing conditions.[17,23] Therefore, the unique chemical composition of CO that mainly comprises carboxyl groups would lead to good stability for proton conductivities. We performed a comparative study on the thermal stability of CO and GO in order to demonstrate the hypothesis. The proton conductivities of CO and GO before and after thermal annealing as a function of RH are shown in Figure 3b. The proton conductivities of GO decreased by 1 and 2 orders of magnitude after thermal annealing at 100 and 140 °C, respectively. In addition, the electronic conductivity of the GO drastically increased following thermal annealing since 120 °C. This observation is in agreement with our previous report; the proton conductivities of GO decrease with decreasing oxygen functional groups and layer distances, while the electron conductivities increase with decreasing oxygen content.[17] Similarly, Sone et al. reported that the proton conductivity of Nafion 117, which is well-known as a good proton conductor and is usually used as a solid electrolyte in fuel cells, decreases after the 110 °C heat treatment.[28] Significantly, for CO, the proton conductivity did not decrease after thermal annealing at 100 °C and retained 50% of the initial activity even after thermal annealing at 200 °C. Moreover, we found that CO was still a perfect electrical insulator after thermal annealing at 200 °C within our experimental conditions.

We further investigated structural and chemical stabilities of CO against thermal annealing. Figure 4 shows the C 1s XPS spectra of CO before and after thermal annealing at various temperatures for 1 h. The chemical composition of CO was almost constant up to 300 °C. Raman spectroscopic analysis (Figure S9) showed that the D- and G-bands at approximately 1350 and 1600 cm^{-1}, respectively, and the D/G intensity ratio as well as the peak positions were almost unchanged upon annealing. TGA curves of CO and GO (Figure S10) revealed a significant weight loss was not observed for the CO sample until 450 °C, while ∼20% weight of the GO sample was lost between 180 and 220 °C because of the release of carbon dioxide from the epoxy group. All these results evidenced that thermally robust proton conductivities of CO come from high thermal stability of carboxyl groups coordinated on CO surfaces.

DOI: 10.1021/acsami.5b06470
ACS Appl. Mater. Interfaces 2015, 7, 23041−23046

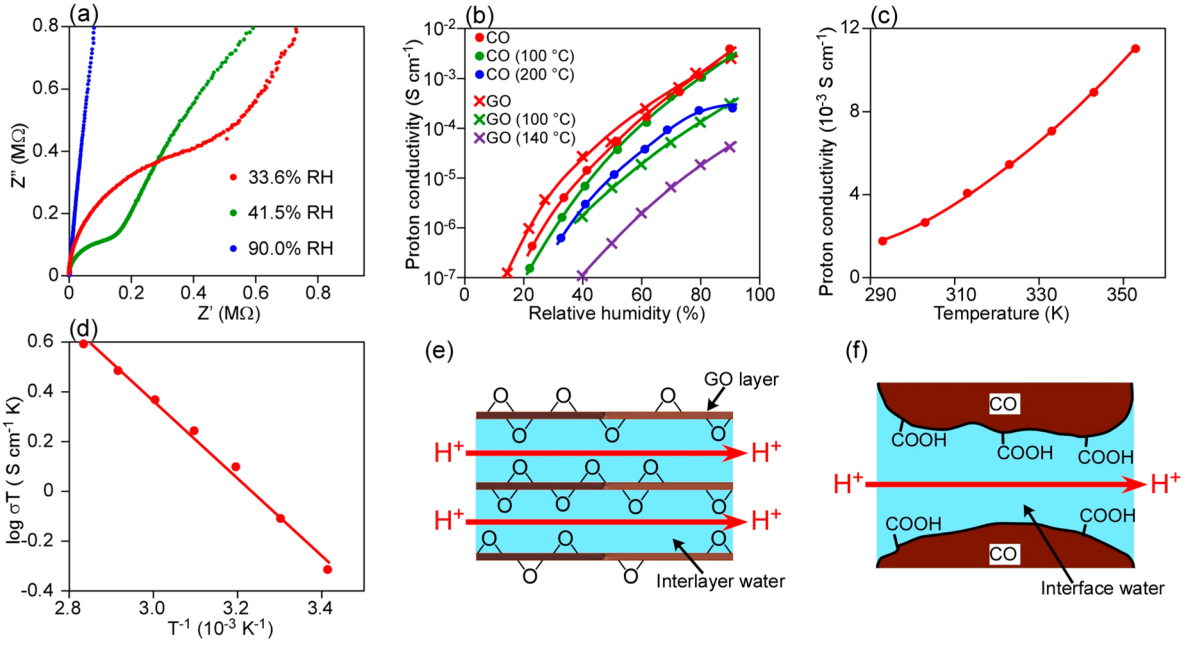

Figure 3. (a) Nyquist plots of CO under various humidified conditions. (b) Proton conductivities of CO and GO as a function of RH at 25 °C. Proton conductivities of CO and GO after thermal annealing at various temperatures for 1 h are also shown. (c) Temperature-dependent proton conductivities and (d) Arrhenius plots of CO at 90% RH. Possible proton conduction mechanism of (e) GO and (f) CO.

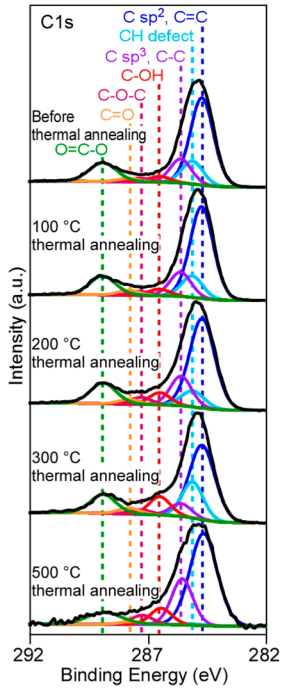

Figure 4. C 1s XPS spectra of CO before and after thermal annealing at various temperatures for 1 h.

3.4. All-Solid-State Electrochemical Capacitor Using CO Electrolyte. An all-solid-state electrochemical capacitor using the GO electrolyte (GOEC) can be produced by a simple method and shows the high capacitance performance and good flexibility.[29,30] However, the electron conductivity generated by the degradation of GO leads to short-circuiting of the electrodes and makes it impossible to use the GOEC. Herein, we replaced GO electrolyte with CO electrolyte to develop a thermally robust all-solid-state electrochemical capacitor. The COEC and GOEC were fabricated by dropping the CO or GO dispersion on the Au comb electrodes and drying in vacuum conditions. A schematic of the fabrication of COEC and GOEC is shown in Figure 5a, and the CCD images of Au comb electrodes before and after production of the COEC are shown in parts b and c, respectively, of Figure 5. CV was measured to evaluate the COEC and GOEC power capabilities, and the results are shown in Figure 6. The nearly rectangular CV shape of COEC indicates that the COEC acts as a double-layer capacitor. The maximum areal capacitance of COEC was ~20 μF cm^{-2} at a scan rate of 1 V s^{-1}; this is higher than the capacitance of GOEC (~10 μF cm^{-2}). We believe that the power capability of COEC can be improved by further development of electrodes beyond the simple gold electrodes used in this study. The COEC showed good thermal stability and exhibited an areal capacitance of ~15 μF cm^{-2} even after thermal annealing at 200 °C. This could not be achieved with GO; the GOEC showed a linear relationship between the potential and current after thermal annealing at 200 °C, indicating the onset of electronic conduction and complete loss of GO activity as a solid electrolyte (Figure S12). Note that, yet, we have not succeeded in the fabrication of a free-standing CO membrane, necessary for some applications such as fuel cells. Nevertheless, as well as modified metal oxide nanoparticles,[22] CO would be utilized as a cost-effective additive to improve the performance of conventional polymer-based membranes owing to similar features including its nanoscale size, high proton conductivity, and high thermal stability.

4. CONCLUSION

In summary, we have successfully fabricated coal oxide by using a simple liquid-phase oxidation process. The CO showed excellent dispersibility in water and had an amorphous structure with a width of ~15−20 nm and a height of ~2−3 nm. XPS analysis showed the presence of many carboxyl groups in CO but scarcely showed any other oxygen functional groups. We

DOI: 10.1021/acsami.5b06470
ACS Appl. Mater. Interfaces 2015, 7, 23041−23046

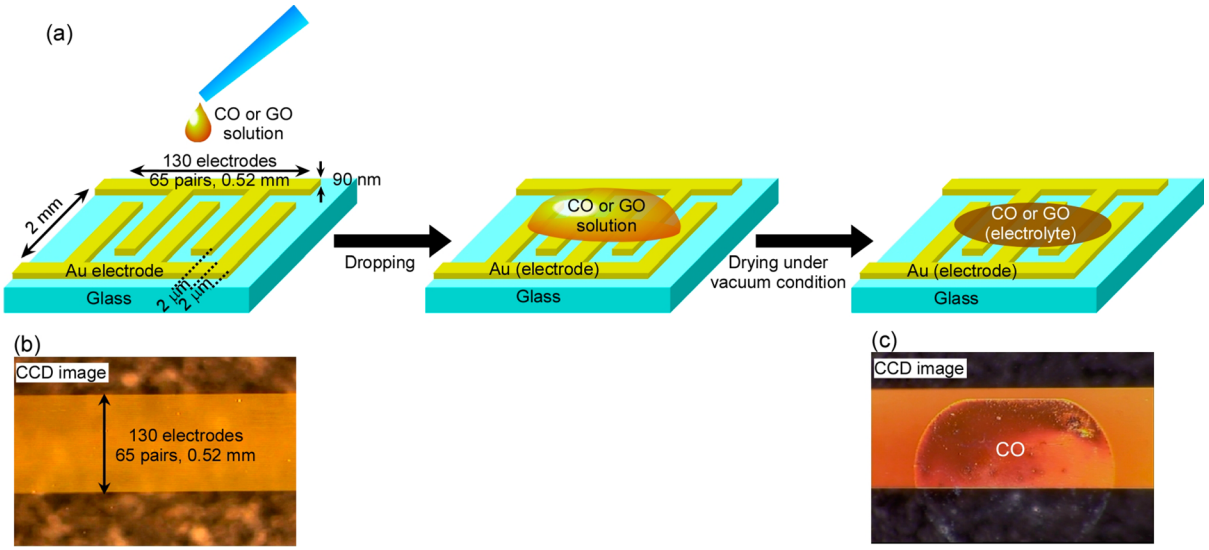

Figure 5. (a) Schematic for the fabrication of COEC and GOEC. CCD images of Au comb electrodes (b) before and (c) after production of COEC.

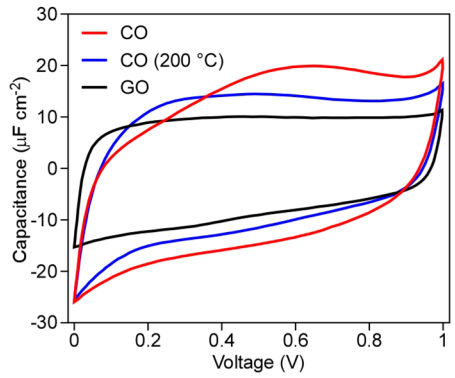

Figure 6. CV curves of COEC and GOEC at a scan rate of 1 V s^{-1}. The result of COEC after thermal annealing at 200 °C is also shown.

also found that the proton conductivity of CO, 3.9 × 10^{-3} S cm^{-1} at 90% RH, is as high as that of GO. Moreover, CO exhibited good thermal stability, with the proton conductivity and capacitance performance of CO changing little even after thermal annealing at 200 °C. The results of our study demonstrate that chemical modification of the widely available coal can be used to obtain proton conductors that can be used in practical applications for a wide range of energy devices.

■ ASSOCIATED CONTENT

Supporting Information

The Supporting Information is available free of charge on the ACS Publications website at DOI: 10.1021/acsami.5b06470.

Experimental details, CCD images, AFM images, SEM images, XRD patterns, UV−vis absorption spectra, FT-IR spectra, Nyquist plots, Raman spectra, TGA data, CV curves (PDF)

■ AUTHOR INFORMATION

Corresponding Authors

*E-mail: kazuto@kumamoto-u.ac.jp (K.H.).
*E-mail: yasumi@gpo.kumamoto-u.ac.jp (Y.M.).

Author Contributions

Y.M. and K.H. designed the experiments and analyzed the data. K.H. and T.T. mainly wrote the manuscript. K.H. and C.O. prepared samples. K.H. evaluated the proton conductivities and capacitance performance and measured AFM, SEM, XRD, Raman, UV−vis, and FT-IR data. C.O. performed TGA measurement. M.K. performed XPS measurements. K.K. performed TEM measurements. S.H. and T.T. made the plane and advised on the optimization of the experiments. All authors discussed and commented on the manuscript. All authors have given approval to the final version of the manuscript.

Notes

The authors declare no competing financial interest.

■ ACKNOWLEDGMENTS

This work was supported by the Core Research of Evolutional Science & Technology (CREST) of the Japan Science, Grant-in-Aid for Challenging Exploratory Research (No. 2365116), Grant-in-Aid for Young Scientists A (No. 15H05411), and Research Fellowships of Japan Society for the Promotion of Science for Young Scientists (No. 15J01300).

■ REFERENCES

(1) Cataldo, F. Polymeric Fullerene Oxide (Fullerene Ozopolymers) Produced by Prolonged Ozonation of C-60 and C-70 Fullerenes. *Carbon* **2002**, *40*, 1457−1467.
(2) Ghosh, S.; Bachilo, S. M.; Simonette, R. A.; Beckingham, K. M.; Weisman, R. B. Oxygen Doping Modifies Near-Infrared Band Gaps in Fluorescent Single-Walled Carbon Nanotubes. *Science* **2010**, *330*, 1656−1659.
(3) Pei, S. F.; Cheng, H. M. The Reduction of Graphene Oxide. *Carbon* **2012**, *50*, 3210−3228.
(4) Chien, C. T.; Li, S. S.; Lai, W. J.; Yeh, Y. C.; Chen, H. A.; Chen, I. S.; Chen, L. C.; Chen, K. H.; Nemoto, T.; Isoda, S.; Chen, M. W.; Fujita, T.; Eda, G.; Yamaguchi, H.; Chhowalla, M.; Chen, C. W. Tunable Photoluminescence from Graphene Oxide. *Angew. Chem., Int. Ed.* **2012**, *51*, 6662−6666.
(5) Eda, G.; Lin, Y. Y.; Mattevi, C.; Yamaguchi, H.; Chen, H. A.; Chen, I. S.; Chen, C. W.; Chhowalla, M. Blue Photoluminescence from Chemically Derived Graphene Oxide. *Adv. Mater.* **2010**, *22*, 505−509.

DOI: 10.1021/acsami.5b06470
ACS Appl. Mater. Interfaces 2015, 7, 23041−23046

(6) Wang, Y.; Huang, Y.; Song, Y.; Zhang, X.; Ma, Y.; Liang, J.; Chen, Y. Room-Temperature Ferromagnetism of Graphene. *Nano Lett.* **2009**, *9*, 220−224.
(7) Taniguchi, T.; Yokoi, H.; Nagamine, M.; Tateishi, H.; Funatsu, A.; Hatakeyama, K.; Ogata, C.; Ichida, M.; Ando, H.; Koinuma, M.; Matsumoto, Y. Correlated Optical and Magnetic Properties in Photoreduced Graphene Oxide. *J. Phys. Chem. C* **2014**, *118*, 28258−28265.
(8) Taniguchi, T.; Tateishi, H.; Miyamoto, S.; Hatakeyama, K.; Ogata, C.; Funatsu, A.; Hayami, S.; Makinose, Y.; Matsushita, N.; Koinuma, M.; Matsumoto, Y. A Self-Assembly Route to an Iron Phthalocyanine/Reduced Graphene Oxide Hybrid Electrocatalyst Affording an Ultrafast Oxygen Reduction Reaction. *Part. Part. Syst. Charact.* **2013**, *30*, 1063−1070.
(9) Matsumoto, Y.; Koinuma, M.; Ida, S.; Hayami, S.; Taniguchi, T.; Hatakeyama, K.; Tateishi, H.; Watanabe, Y.; Amano, S. Photoreaction of Graphene Oxide Nanosheets in Water. *J. Phys. Chem. C* **2011**, *115*, 19280−19286.
(10) Joshi, R. K.; Carbone, P.; Wang, F. C.; Kravets, V. G.; Su, Y.; Grigorieva, I. V.; Wu, H. A.; Geim, A. K.; Nair, R. R. Precise and Ultrafast Molecular Sieving Through Graphene Oxide Membranes. *Science* **2014**, *343*, 752−754.
(11) Li, H.; Song, Z. N.; Zhang, X. J.; Huang, Y.; Li, S. G.; Mao, Y. T.; Ploehn, H. J.; Bao, Y.; Yu, M. Ultrathin, Molecular-Sieving Graphene Oxide Membranes for Selective Hydrogen Separation. *Science* **2013**, *342*, 95−98.
(12) Kim, H. W.; Yoon, H. W.; Yoon, S. M.; Yoo, B. M.; Ahn, B. K.; Cho, Y. H.; Shin, H. J.; Yang, H.; Paik, U.; Kwon, S.; Choi, J. Y.; Park, H. B. Selective Gas Transport Through Few-Layered Graphene and Graphene Oxide Membranes. *Science* **2013**, *342*, 91−95.
(13) Hatakeyama, K.; Karim, M. R.; Ogata, C.; Tateishi, H.; Funatsu, A.; Taniguchi, T.; Koinuma, M.; Hayami, S.; Matsumoto, Y. Proton Conductivities of Graphene Oxide Nanosheets: Single, Multilayer, and Modified Nanosheets. *Angew. Chem., Int. Ed.* **2014**, *53*, 6997−7000.
(14) Gao, W.; Wu, G.; Janicke, M. T.; Cullen, D. A.; Mukundan, R.; Baldwin, J. K.; Brosha, E. L.; Galande, C.; Ajayan, P. M.; More, K. L.; Dattelbaum, A. M.; Zelenay, P. Ozonated Graphene Oxide Film as a Proton-Exchange Membrane. *Angew. Chem., Int. Ed.* **2014**, *53*, 3588−3593.
(15) Karim, M. R.; Hatakeyama, K.; Matsui, T.; Takehira, H.; Taniguchi, T.; Koinuma, M.; Matsumoto, Y.; Akutagawa, T.; Nakamura, T.; Noro, S.; Yamada, T.; Kitagawa, H.; Hayami, S. Graphene Oxide Nanosheet with High Proton Conductivity. *J. Am. Chem. Soc.* **2013**, *135*, 8097−8100.
(16) Kim, S.; Zhou, S.; Hu, Y. K.; Acik, M.; Chabal, Y. J.; Berger, C.; de Heer, W.; Bongiorno, A.; Riedo, E. Room-Temperature Metastability of Multilayer Graphene Oxide Films. *Nat. Mater.* **2012**, *11*, 544−549.
(17) Hatakeyama, K.; Tateishi, H.; Taniguchi, T.; Koinuma, M.; Kida, T.; Hayami, S.; Yokoi, H.; Matsumoto, Y. Tunable Graphene Oxide Proton/Electron Mixed Conductor that Functions at Room Temperature. *Chem. Mater.* **2014**, *26*, 5598−5604.
(18) Hook, M.; Zittel, W.; Schindler, J.; Aleklett, K. Global Coal Production Outlooks Based on a Logistic Model. *Fuel* **2010**, *89*, 3546−3558.
(19) Ye, R. Q.; Xiang, C. S.; Lin, J.; Peng, Z. W.; Huang, K. W.; Yan, Z.; Cook, N. P.; Samuel, E. L. G.; Hwang, C. C.; Ruan, G. D.; Ceriotti, G.; Raji, A. R. O.; Marti, A. A.; Tour, J. M. Coal as an Abundant Source of Graphene Quantum Dots. *Nat. Commun.* **2013**, *4*, 2943.
(20) Fei, H. L.; Ye, R. Q.; Ye, G. L.; Gong, Y. J.; Peng, Z. W.; Fan, X. J.; Samuel, E. L. G.; Ajayan, P. M.; Tour, J. M. Boron- and Nitrogen-Doped Graphene Quantum Dots/Graphene Hybrid Nanoplatelets as Efficient Electrocatalysts for Oxygen Reduction. *ACS Nano* **2014**, *8*, 10837−10843.
(21) Ye, R. Q.; Peng, Z. W.; Metzger, A.; Lin, J.; Mann, J. K.; Huang, K. W.; Xiang, C. S.; Fan, X. J.; Samuel, E. L. G.; Alemany, L. B.; Marti, A. A.; Tour, J. M. Bandgap Engineering of Coal-Derived Graphene Quantum Dots. *ACS Appl. Mater. Interfaces* **2015**, *7*, 7041−7048.
(22) Aslan, A.; Bozkurt, A. Nanocomposite Membranes Based on Sulfonated Polysulfone and Sulfated Nano-Titania/NMPA for Proton Exchange Membrane Fuel Cells. *Solid State Ionics* **2014**, *255*, 89−95.
(23) Koinuma, M.; Ogata, C.; Kamei, Y.; Hatakeyama, K.; Tateishi, H.; Watanabe, Y.; Taniguchi, T.; Gezuhara, K.; Hayami, S.; Funatsu, A.; Sakata, M.; Kuwahara, Y.; Kurihara, S.; Matsumoto, Y. Photochemical Engineering of Graphene Oxide Nanosheets. *J. Phys. Chem. C* **2012**, *116*, 19822−19827.
(24) Dimiev, A. M.; Tour, J. M. Mechanism of Graphene Oxide Formation. *ACS Nano* **2014**, *8*, 3060−3068.
(25) Koinuma, M.; Tateishi, H.; Hatakeyama, K.; Miyamoto, S.; Ogata, C.; Funatsu, A.; Taniguchi, T.; Matsumoto, Y. Analysis of Reduced Graphene Oxides by X-ray Photoelectron Spectroscopy and Electrochemical Capacitance. *Chem. Lett.* **2013**, *42*, 924−926.
(26) Dreyer, D. R.; Park, S.; Bielawski, C. W.; Ruoff, R. S. The Chemistry of Graphene Oxide. *Chem. Soc. Rev.* **2010**, *39*, 228−240.
(27) Agmon, N. The Grotthuss Mechanism. *Chem. Phys. Lett.* **1995**, *244*, 456−462.
(28) Sone, Y.; Ekdunge, P.; Simonsson, D. Proton Conductivity of Nafion 117 as Measured by a Four-Electrode AC Impedance Method. *J. Electrochem. Soc.* **1996**, *143*, 1254−1259.
(29) Gao, W.; Singh, N.; Song, L.; Liu, Z.; Reddy, A. L. M.; Ci, L. J.; Vajtai, R.; Zhang, Q.; Wei, B. Q.; Ajayan, P. M. Direct Laser Writing of Micro-Supercapacitors on Hydrated Graphite Oxide Films. *Nat. Nanotechnol.* **2011**, *6*, 496−500.
(30) El-Kady, M. F.; Strong, V.; Dubin, S.; Kaner, R. B. Laser Scribing of High-Performance and Flexible Graphene-Based Electrochemical Capacitors. *Science* **2012**, *335*, 1326−1330.

DOI: 10.1021/acsami.5b06470
ACS Appl. Mater. Interfaces 2015, 7, 23041−23046